Journal of MATERIALS RESEARCH

Article
DOI:10.1557/s43578-023-00941-x

Defect-free ZnO nanorods with high angular distribution for enhanced excitonic emission

Saskia Fiedler[1,2], Cuong Ton-That[2,a], Matthew R. Phillips[2]

[1] Federal Institute for Materials Research and Testing, 1.2 Biophotonics, Richard-Willstätter-Str. 11, 12489 Berlin, Germany
[2] School of Mathematical and Physical Sciences, University of Technology Sydney, 15 Broadway, Ultimo, NSW 2007, Australia
[a] Address all correspondence to this author. e-mail: Cuong.Ton-That@uts.edu.au

Received: 12 December 2022; accepted: 13 February 2023; published online: 8 March 2023

Low-temperature hydrothermal growth has emerged as a popular method for the fabrication of ZnO nanorods (NRs), increasing the functionality and utility of ZnO-based devices. In this work, we study the influence of growth time, temperature and seed layer on the dimensions and angular distribution of ZnO NRs. High-quality NRs with a crisscrossed 60° angular distribution have been grown with a 20–60 nm diameter and 600 nm length. We show that, within the ideal range of growth parameters, the growth time and temperature have no controllable influence on NR diameter and length, while the deposition method and size of the pre-growth deposited ZnO seeds affects diameter and NR angular alignment. We demonstrate advantages of using crisscross-aligned NRs over planar ZnO for the enhancement of ZnO excitonic emission by optical coupling with gold nanoparticles. These results can be readily adapted for applications that involve surface coating-mediated enhancement of both light emission and injection.

Introduction

Zinc oxide (ZnO), occurring mainly in a hexagonal wurtzite structure [1], is an attractive, non-toxic, chemically stable wide bandgap semiconductor ($E_g = 3.37$ eV) owing to its technologically useful opto-electronic properties [2, 3]. Significantly, ZnO can be easily grown in a variety of bespoke nanostructures [2, 4, 5] which typically provide different but controllable optical and mechanical properties when compared with their bulk counterparts. Consequently, bulk and nanostructured ZnO, in particular ZnO nanorods (NRs), can be used in a broad range of practical electronic devices, such as LEDs, laser diodes, photovoltaics, photodetectors and chemical sensors [6–14]. However, many applications require precise control over the dimensions of the ZnO NRs. While this goal can be achieved by a number of different growth techniques [15–18], most of these approaches are expensive and often difficult to scale up. In addition, many of the growth techniques involving physical and chemical deposition methods use high temperatures [19] which can often limit or degrade the electrical and optical properties of ZnO NR-based devices. Accordingly, Greene et al. [20] proposed a cost-effective and large-scale hydrothermal method for the growth of ZnO NRs at very low temperatures around 90 °C with a preferential growth direction along the *c*-axis [21–23]. Significantly, low temperature fabrication also enables ZnO NR fabrication on flexible substrates, such as thermally sensitive organic materials, considerably increasing the utility and functionality of ZnO devices and their applications [24]. Due to the distinct advantages of the low temperature hydrothermal technique, this method has been extensively studied to understand the fundamental growth mechanisms to precisely control the morphology and size of the ZnO NRs [25]. Despite this effort, there still seems to be little agreement on which growth parameters are principally responsible for determining the spatial dimensions of the ZnO NRs. While some papers report that increasing the growth time results in longer and thicker hexagonal ZnO NRs [20, 26–28], others conversely observed that only the NR length increased without either a diameter change [29] or a modification in morphology [30]. Similar controversy in the literature exists about the use of the growth temperature to tune diameter and/or length of NRs. For example, Xu et al. [31] found that the growth temperature had the largest effect on the NR aspect ratio with the optimum aspect ratio occurring at 70 °C, while higher temperatures resulted in pyramid-like nanostructures. Nandi et al. [32], however, observed that increasing the growth temperature from 70 to 90 °C only affected the NR length but not the diameter, while only a change of morphology

was found by Al-lami and Jaber [33]. Hydrothermal growth of ZnO NRs conventionally uses a ZnO seed layer on the substrate before growth to promote a higher density and a better coverage of NRs. This ZnO seed layer is generally deposited by a broad range of techniques such as sputter-coating, drop-casting and spin-coating nanoparticles. These techniques collectively produce a wide range of different as-grown pre-treated substrate types [32, 34–39]. Therefore, it is important and relevant to study and understand the effects that the ZnO seed layer and the other growth parameters have on the degree of control over the morphology and dimensions of ZnO NRs, and to determine the reproducibility of these results.

The great interest in the control over and reproducibility of the morphology, dimension and alignment of ZnO NRs is mainly due the outstanding optical properties of ZnO NRs and their potential use for various opto-electronic applications and devices. Special emphasis has been paid to the enhancement of the excitonic emission in the UV and the reduction/suppression of the defect-related visible emission (DL) or an overall increase of UV-to-DL ratio. It has been repeatedly reported that surface coatings, particularly those consisting of metal thin films or metal nanoparticle (NP), can significantly enhance the UV emission of ZnO NRs (and other nanostructures) [40–47]. Due to its ease of fabrication and its inertness, Au NP-coatings have been studied intensively by many researchers, including us, achieving a moderate excitonic emission enhancement in ZnO NRs [46, 48–50]. Although the enhancement mechanism of Au NP-coated ZnO NRs has been attributed to different underlying effects—such as plasmonic coupling, energy- and (hot) electron-transfer, increase of spontaneous emission rate via an additional recombination channel—this article does not attempt to repeat any of the existing studies but rather aims to demonstrate the general advantage of using ZnO NRs with high angular orientation for metal NP-coating-mediated enhancement. In the first part of this work, we present a systematic study of the influence of the ZnO seed layer, using a drop-casting deposition and sputter-coating technique, on the morphology of hydrothermally grown ZnO NRs. Additionally, we investigate the tunability of NR length and diameter by systematically varying growth time and temperature within a narrow window of 2–4 h and a temperature ranging from 70 to 100 °C [20, 32, 51]. The rationale behind the selection of this small variation in growth parameters is twofold: (i) the growth of hexagonal, thin ZnO NRs has been repeatedly reported to be within this range of growth parameters; (ii) such a slight change in growth parameters allows to gain insight in the reproducibility and the actual tunability of the dimensions of hydrothermally grown ZnO NRs which is of paramount importance for industrial implementation of this growth method.

We find that both the length and diameter of hydrothermally grown ZnO NRs vary considerably between batches using the exact same growth conditions. The seed layer is found to be important in ensuring homogeneous coverage of the ZnO NRs, however, the size of drop-casted seeds does not significantly influence the diameter of the resulting NRs. Instead, the diameter of the NR is observed to range from 20 to 60 nm with an approximate length of 600 nm regardless of the seed layer properties or the chosen growth parameters. We further demonstrate that a sputter-coated ZnO seed layer exerts a major influence over the diameter of the grown ZnO NRs and their angular distribution with respect to the substrate. The coverage and density of ZnO seeds for both methods result in a controllable angular/vertical alignment of the hydrothermally grown ZnO NRs. This result is useful for application realizations such as wave-guiding, angular distributions of light-emitting profiles and sensing.

In the second part of this article, we study the optical properties of the hydrothermally grown ZnO NRs and present a method to enhance the UV emission in ZnO. We show that the as-grown ZnO NRs exhibit exceptional crystallinity with almost exclusive UV emission and close to no defect-related (DL) emission. For both types of excitations—photons and electrons—we achieve a high UV-to-DL ratio with up to 50. Furthermore, we demonstrate an up to 5.1-fold enhanced UV emission by applying an Au NP surface coating. This extraordinary optical enhancement is achieved by exploiting the wide angular distribution of the hydrothermally grown ZnO NRs. The random NR network allows for: (i) an excellent surface coverage without shadowing effects using a simple sputter-deposition of Au NPs, and (ii) a more effective (photo- or electron-beam) excitation due to larger surface areas facing the top of the sample, facilitating a larger emission enhancement of the NRs. We confirm (ii) by applying an identical Au NP-coating onto planar ZnO substrates, exhibiting an enhancement factor of only up to 2. ZnO NRs with high angular distribution can therefore be used in conjunction with surface coatings for light emission or light extraction enhancement/management of light-emitting or photovoltaic applications and devices.

Results and discussion

Control of the dimensions and alignment of hydrothermally grown ZnO NRs

Influence of growth time on the dimension of ZnO NRs

To study the effect of growth time on the dimensions of ZnO NRs, Si substrates with a pre-growth drop-casted seed layer were used for hydrothermal growth at a temperature of 90 °C. Figure 1(a–e) shows SEM images at 10 kV of the ZnO NRs hydrothermally grown for 2–4 h in 0.5 h steps. The NRs are observed to grow outward from the substrate with a random angular distribution between 0 and ~ 30° with respect to the surface normal while the diameter ranges approximately from

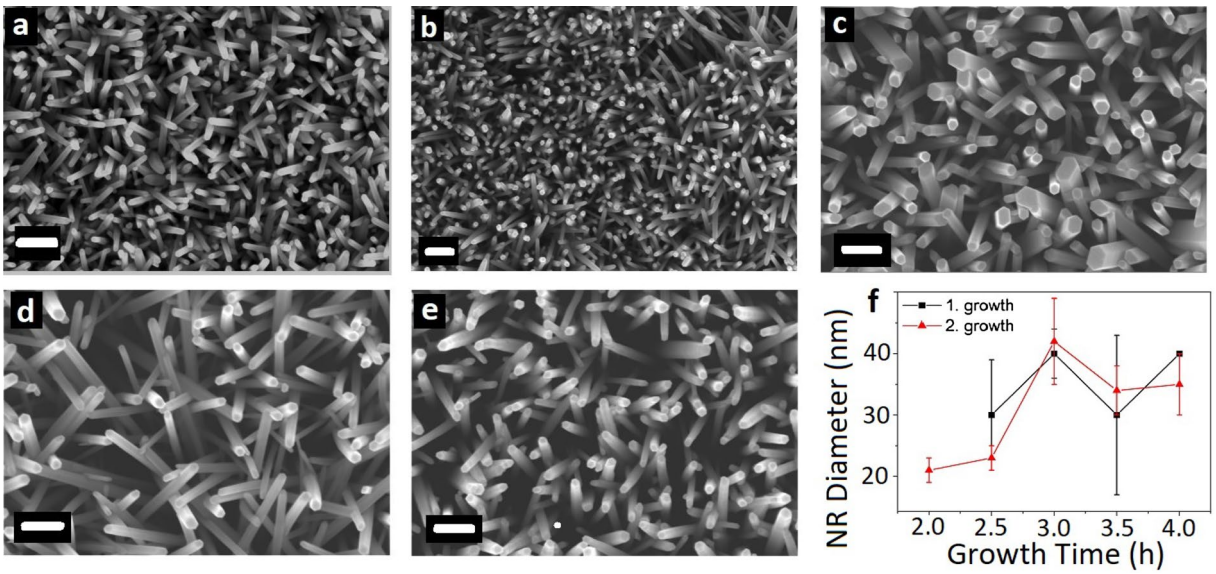

Figure 1: SEM images of hydrothermally grown ZnO nanorods grown at 90 °C for (a) 2 h, (b) 2.5 h, (c) 3 h, (d) 3.5 h and (e) 4 h. The scale bare denotes 200 nm. (f) NR diameter, averaged over 50 NRs, together its standard deviation, as a function of growth time for two separate growth runs.

20 to 50 nm depending on growth time. The NR diameter versus growth time is depicted in Fig. 1(f). Here the mean diameter of the grown ZnO NRs is determined by measuring 50 typical NRs from the calibrated SEM images of each sample and the error bar represents one standard deviation. Despite the large error bars, representing a larger distribution of NR diameters for some of the samples, the set of samples from the first growth run for 2–4 h show an increasing trend for 2–3 h followed by a decrease of diameter. Although exhibiting similar diameters, a second set of ZnO NR samples grown under the same growth conditions with identically prepared substrates do not have an identical profile to run one. Note that at a growth time of 2 h in the first run, no ZnO NRs were grown. While the origin of this discrepancy between run one and two is unclear, it has been reported that the temperature plays an essential role in the rate of chemical reactions and therefore, the nucleation and growth rate is enhanced when the temperature is increased [25]. Potentially, a growth temperature of 70 °C is close to the required minimum for nucleation, probably resulting in a fine line between growth and no-growth of ZnO NRs. The comparison of the diameter of ZnO NRs grown at longer times reveals an average diameter of 40 ± 15 nm and 35 ± 5 nm in run one and two, respectively. Larger ZnO rods with diameters of a few of 100 s of nanometers formed from merged nanorods were found in all growth experiments but were disregarded in this study [52].

The observed non-vertical orientation of the ZnO NRs (see Figs. 1 and S1) seems to randomly vary from sample to sample, indicating that the growth time cannot be used to control the angular distribution. Further discussion on the NR alignment will follow in the section of the effect of the seed layer. The length of the NRs is also found to vary between 500 and 700 nm for all samples (see Fig. S1a), regardless of growth temperature, time and the seed layer.

Influence of growth temperature on the dimensions of ZnO NRs

To investigate the effect of growth temperature on the NR dimensions, a set of samples were grown at different temperatures ranging from 70 to 100 °C for 2 to 4 h in 0.5 h increments, keeping all other conditions constant with identically prepared substrates. Figure 2(a) and (b) show the average diameter of ZnO NRs at each growth temperature versus growth time for two separate growth runs, one and two, respectively. The first set of samples, shown in Fig. 2(a), reveals that the average diameter of NRs grown at each temperature is relatively constant over the entire range of growth time with an exception for NRs grown at 100 °C, stressing again the lack of NR size control via growth time. Similarly, the NR diameter cannot be reproducibly tuned by varying the growth temperature as noted in the table in Fig. 2(c).

Although a precise tunability of the NR diameter via growth time or temperature cannot be achieved, a relatively small (average) diameter for all hydrothermally grown ZnO NRs was observed. In fact, most reports, which use a similar approach of hydrothermal growth, show ZnO rods with an average diameter well above 100 nm [53–55].

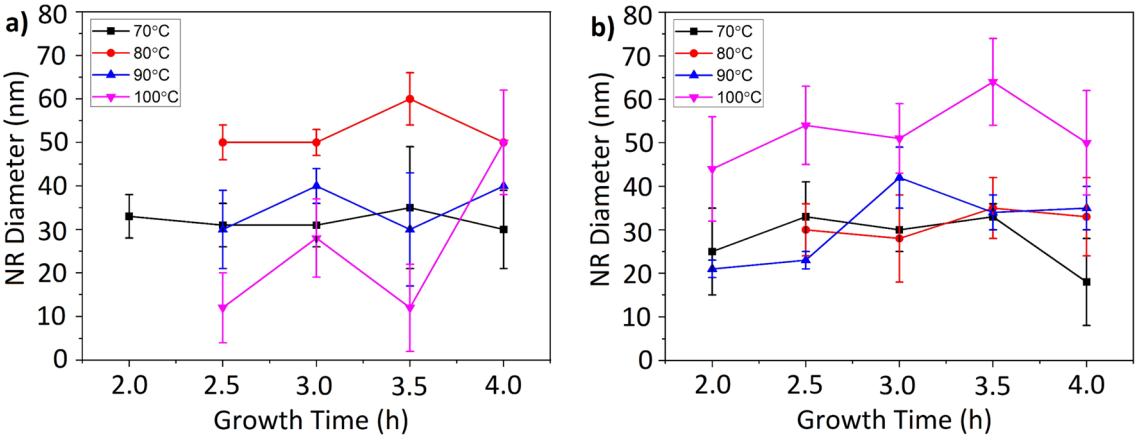

c)

	70°C	80°C	90°C	100°C
Run 1	32±3	53±7	25±15	25±15
Run 2	28±5	32±3	32±12	42±12

Figure 2: Average diameter of ZnO nanorods grown at 70, 80, 90, 100 °C versus growth time ranging from 2 to 4 h in 0.5 h steps. (a) and (b) Results of two separate ZnO nanorod growth runs under the same conditions. (c) Summary of resulting ZnO NR diameters.

Influence of drop-casted and sputter-coated seed layers on ZnO NR diameter

To study the effect of pre-growth seed layer, two different seed layers—drop-casting of zinc acetate and sputter-coating of ZnO nanocrystals—have been applied to the substrate before the ZnO NR growth. First, we drop-casted zinc acetate solution onto the Si substrate multiple times and subsequently annealed at 250 °C for 20 min. This entire procedure was repeated several times. All deposited seed layers were continuous and evenly distributed across the substrate. In all of these pre-growth SEM studies, no significant differences in morphology of the seed layers or peel-off effects were observed, indicating that the seed layer deposition is highly reproducible. However, it is noteworthy that close to no NRs were grown on a substrate without a seed layer—a few thick or flower-like ZnO structures were found, potentially nucleated at defects of the otherwise clean substrate.

Figure 3 shows the morphology of three different (drop-casted) seed layers, as described in the caption, as well as the resulting ZnO NRs grown hydrothermally at 90 °C for 3 h. Figure 3(a–c) shows the SEM images of seed layer 1 and the as-grown ZnO NRs. Large areas of the substrate are evenly covered with seeds of an average diameter of 80 ± 15 nm. Interestingly, the seed layer 2, shown in the second row of Fig. 3(d–f), is less homogenously distributed over the substrate, while the seeds have a slightly bigger average diameter of 100 ± 20 nm. The seed layer 3, displayed in the bottom row of Fig. 3(g–i), resulted in a poorer coverage than that of seed layer 1 and 2. The higher magnification image [cf. Fig. 3(h)] shows that the seeds have merged together with an average diameter of 150 ± 20 to 200 ± 25 nm. Additionally, dark and bright patches in the SE images are visible which is consistent with electron-beam-induced charging, indicating that this seed layer is poorly conducting compared with the two other seed layers [cf. Fig. 3(b, e)]. Therefore, no high-magnification SE image of the seed layer 3 could be collected due to the charging effect. The ZnO NRs hydrothermally grown at 90 °C for 3 h onto the three different seed layers are depicted in the right column of Fig. 3(c, f, i). The ZnO NRs grown on seed layer 1 exhibit a hexagonal shape with a mean diameter of 35 ± 7 nm. Additionally, a number of larger NRs with an average diameter of 55 ± 10 nm is found. As expected from the dense layer of seeds, the coverage of the ZnO NRs is very good; their vertical alignment, however, exhibits a range of angles in all directions with respect to the substrate surface normal between approximately 0 and 60°. Surprisingly, the ZnO NRs grown on seed layer 2 look very similar to that grown on seed layer 1. Two sizes of hexagonal NRs are found, 35 ± 12 and 50 ± 10 nm. Compared with seed layer 1, the coverage over the substrate with seed layer 2 is around 80% with a slightly more vertical alignment of NRs over a smaller range of angles from approximately 0 and 45°. In addition, some areas show flower-like clusters of ZnO NRs, most likely grown from bigger isolated seeds, as displayed in the inset of Fig. 3(f). Seed layer 3 resulted in growth of hexagonal ZnO NRs with a larger variation in diameter ranging from 30 to 70 nm. These NRs exhibit a larger angular distribution with respect to the substrate normal than both seed layer 1 and 2, resulting in strong NR crisscrossing. A

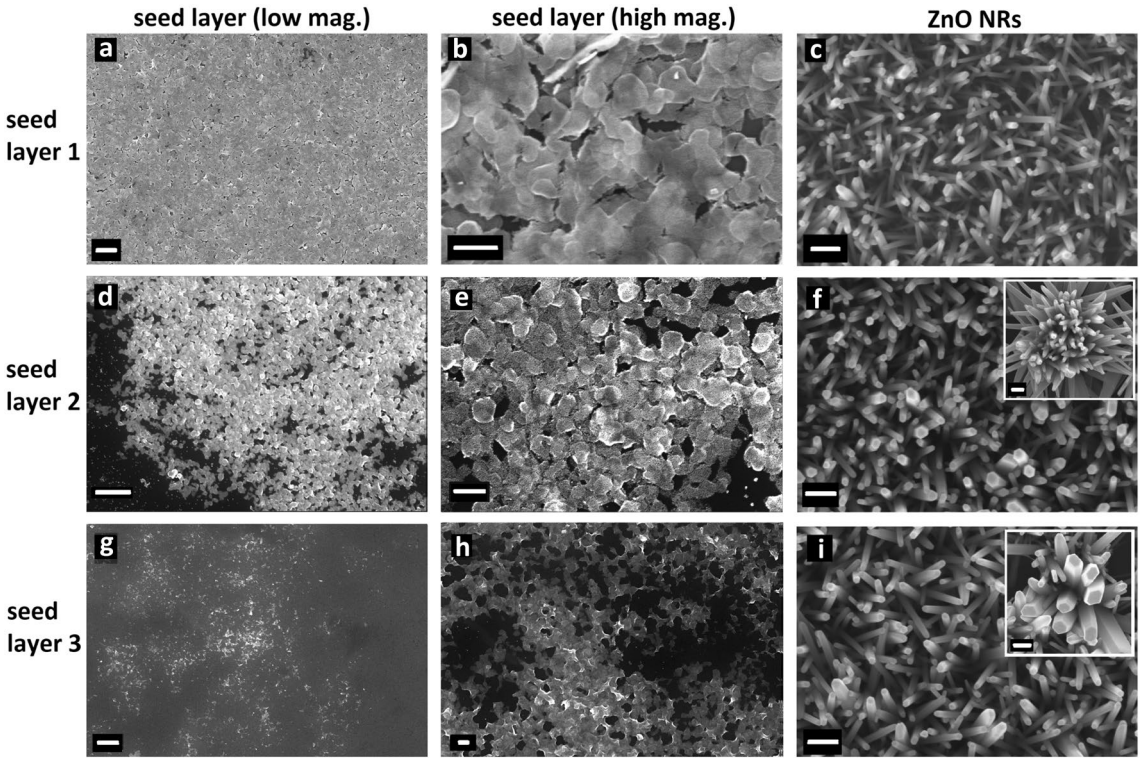

Figure 3: Comparison of three different ZnO seed layers for hydrothermal growth of ZnO nanorods at 90 °C for 3 h; top to bottom: (1) five times drop-casted and annealing twice, (2) five times drop-casted and annealing three times, and (3) ten times drop-cast and annealing twice. The left column (a, d and g) shows the SEM images of the seed layers 1–3 at low magnification, while the SEM images in the center column (b, e and h) were collected at high-magnification. The right column (c, f and i) displays the SEM images of the resulting hydrothermally grown ZnO nanorods. The scale bar is 1000 nm in the left column, and 200 nm in the center and right columns, including the insets.

few flower-like NR clusters are also present [cf. inset of Fig. 3(i)]. Our results reveal that the number of times the zinc acetate solution was drop-casted onto the substrate and the repetition of the drop-casting and annealing cycle both have virtually no effect on the morphology and the diameters of the hydrothermally grown ZnO NRs. Additionally, while the coverage of the seeds over the substrate is essential for homogeneous growth of ZnO NRs, the average seed size appears to have no effect on the as-grown average NR diameter. Furthermore, it appears that a smoother and more uniform surface coating by the ZnO seeds may facilitate growth of flower-like NR clusters, suggesting that the NRs grow from cracks, edges or irregularities as well as from the grain boundaries of the seeds. This rather random nucleation may also explain the large angular distribution of the NRs with respect to the substrate normal, which is opposite to the suggestion in literature that larger diameter seeds might favor surface nucleation [56, 57]. In fact, Chen et al. [57] reports that grain-boundary nucleation typically results in a high angular distribution of NRs.

Sputter-coated ZnO layers with two different nominal thicknesses of 2 and 5 nm were used as seeded substrate for hydrothermal ZnO NR growth at 90 °C for 3 h, as displayed in Fig. 4. In both cases, well-separated seeds were deposited with a relatively smaller size of 30–40 nm than the drop-casted seed layers shown in Fig. 3. The first row of Fig. 4 reveals that the layer with a nominal thickness of 2 nm exhibits a uniform distribution of ZnO seeds without any agglomerations. The resulting ZnO NRs, shown in Fig. 4(b, c), possess an average diameter of 30 ± 7 nm, similar to the diameter of the ZnO seeds on the substrate, with an angular distribution relative to the substrate of up to 60°. While the ZnO layer at a longer sputtering time, displayed in the bottom row of Fig. 4, resulted in seeds with a similar size, however, some have merged to form larger seeds and have a lower density compared with the seed layer prepared with a shorter sputtering time [cf. Fig. 4(d)]. Consequently, the size distribution of as-grown ZnO NRs diameter is broadened, ranging from 30 to 100 nm, indicating that the spatial dimension of the seeds mediates the diameter of the NRs. Accordingly, using sputter-coated ZnO nanocrystals as a seed layer for hydrothermal NR growth can provide some control over the NR diameter, which was not the case with the drop-casting method. This is in agreement with the different types of nucleation, grain-boundary and surface nucleation, respectively, for the two methods of seed layer deposition, drop-casting and sputter-coating.

Some of the thicker NRs exhibit a tapered morphology, which could be due to overgrowth of smaller NRs during the growth process. Significantly, the angle of these NRs with respect

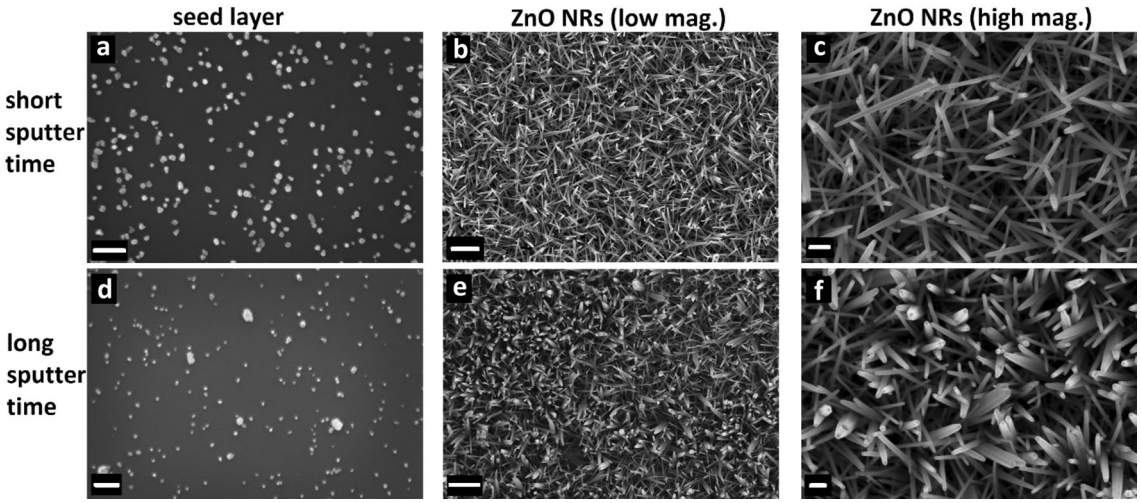

Figure 4: Sputter-coated ZnO as seeds for hydrothermal ZnO NR growth (90 °C for 3 h). SE images at 10 kV of nominally (a–c) 2 nm and (d–f) 5 nm sputter-coated ZnO onto Si substrate and resulting ZnO NRs at low (b and e) and high-magnification (c and f). The scale bar in the left and right columns denotes 200 nm, while it is 1000 nm in the center panels.

to the substrate normal is much smaller ranging up to 30° than the shorter sputtering time seed layer. This reduction in the NR angular distribution is most likely the result of the thicker NRs grown on the second ZnO seed layer occupying more space on the substrate, limiting the spread of growth angles. These results show that the size of the ZnO seed can be also used to regulate the angular distribution of the NRs.

Optical properties of hydrothermally grown ZnO NRs and UV emission enhancement

Luminescence and XRD characterization of as-grown ZnO NRs

X-ray Diffraction (XRD) data as well as cathodoluminescence (CL) and photoluminescence (PL) spectra were collected from representative ZnO NRs hydrothermally grown at 90 °C for 3 h on a drop-casted seeded substrate. The XRD results confirm that the ZnO NRs grow preferentially along the c-axis, as depicted in Fig. 5(a) with a single-crystalline hexagonal wurtzite crystal structure free of any impurity phases. Figure 5(b) displays a typical CL spectrum at 10 K revealing a sharp, intense near-band-edge (NBE) peak in the UV spectral range, attributed to free (FX) and donor-bound (DBX) excitons. A representative high-resolution PL spectrum showing FX and DBX emission with their phonon replicas LO-FX and LO-DBX as well as the ZnO A-band and a two-electron satellite (TES) peak is depicted in Fig. 5(c) [1, 58]. Additionally, the appearance of FX and DBX as well as their phonon replicas in the measured PL spectra in Fig. 5(c) provides strong evidence that the ZnO NRs have a high crystalline quality [59]. The CL and PL studies also found no evidence of contamination or the presence of

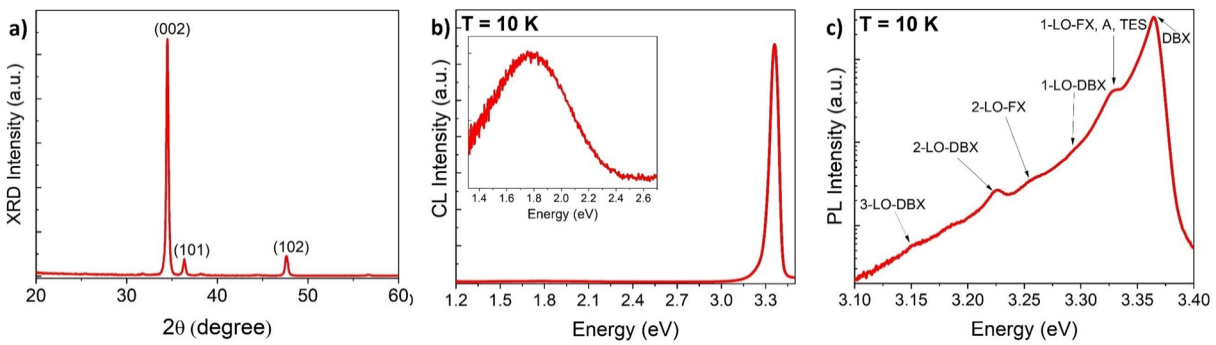

Figure 5: (a) A typical XRD spectrum of as-grown hydrothermal ZnO NRs showing that NRs have a hexagonal wurtzite structure, and that the growth is predominately along the *c*-axis. (b) CL spectra at 3 kV of hydrothermally grown ZnO NRs (90 °C for 3 h) at 10 K, showing the characteristic intense, sharp UV emission of the NBE and the very weak and broad defect-related DL emission at 1.8 eV. The inset shows the DL emission, centered at 1.8 eV. (c) High-resolution PL spectrum of the NBE emission showing signature emission for FX phonon replica 2-LO-FX, DBX and its phonon replicas LO-DBX, ZnO A-band and a two-electron satellite band.

extended structural defects in the ZnO NRs. The CL spectrum in Fig. 5(b) with enlarged visible range in the inset exhibits a very weak and broad deep-level (DL) emission at 1.8 eV which is widely attributed to native vacancy point defects in the bandgap that act as radiative recombination centers [60, 61]. Interestingly, green luminescence which is commonly found in ZnO nanostructures and ascribed to oxygen vacancies [62], is absent in these samples, indicating that the as-grown ZnO NRs are rather oxygen-rich than depleted in oxygen. A UV-to-DL ratio of more than 50 was found, confirming the exceptionally high crystal and luminescence quality of those sub-100 nm-thin ZnO NRs which was found to be reproducible and independent on the growth parameters chosen for this study.

UV emission enhancement using Au nanoparticle surface coating

The high crystal and luminescence quality of the ZnO NRs in combination with their large angular distribution make them a promising candidate for applications involving light enhancement or light injection/extraction. In particular, the crisscross alignment of the ZnO NRs is advantageous for the decoration with various surface coatings as the surface area is easily accessible for spatially uniform deposition of thin films. Furthermore, the accessibility of the surface area also allows for its effective optical (or electron-beam) excitation and light emission collection. We used Au sputter-deposition and annealing to produce a uniform Au NP-coating onto the hydrothermally grown ZnO NRs (inset of Fig. 6). The UV enhancement mechanism in these samples has been previously attributed to the creation of an additional, faster relaxation channel through non-radiative (interband) transitions in Au, increasing the UV spontaneous emission rate [46]. It is expected that any changes in the spectral shape of the ZnO emission, particularly defect emission, will not affect the Au NP-mediated UV enhancement, allowing us to compare highly crisscross-aligned ZnO NRs with planar ZnO substrates (*a*-plane). The inset of Fig. 6 demonstrates the uniformity of the Au NP surface coating over a large area of a thick ZnO NR. The average diameter of the Au NP is 5 nm, excluding potential quantum confinement effects in these samples.

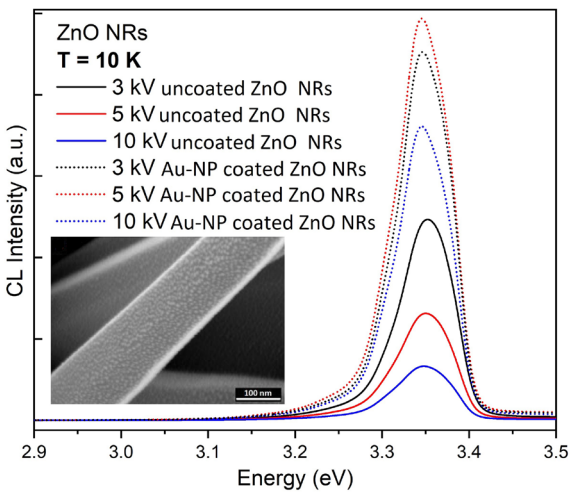

Figure 6: Depth-resolved CL spectra of uncoated (solid) and Au NP-coated (dotted) ZnO NRs collected at 10 K. Inset shows the SEM image of a thick ZnO NR decorated with 5 nm-sized Au NPs. The scale bar denotes 100 nm.

First, we study the UV enhancement factor of the Au NP-coated ZnO NRs using electron-beam excitation. The advantage of CL over PL spectroscopy is the possibility to control the probing depth of the incoming electrons into the sample by varying the acceleration voltage (HV). In Fig. 6, CL spectra of uncoated and Au NP-coated ZnO NRs are displayed using an HV of 3, 5 and 10 kV which translates to a probing depth of approximately 50, 100 and 350 nm, respectively. The resulting UV enhancement factor up to 5.1 is found to be highly dependent on the probing depth (Table 1). Interestingly, the UV enhancement increases with increasing probe depth, opposed to the intuition that the interaction between the Au NPs and ZnO is greatest near their interface.

To further study this depth-dependent trend in UV enhancement due to the Au NP surface coating, Monte Carlo simulations were performed [63]. For simplicity, the electron energy loss (EEL) profile was simulated for bulk ZnO coated with a 5 nm Au film, while additionally drawn white lines in Fig. 7 mimic the ZnO NRs with a diameter of 40 nm. Although the actual orientation of the hydrothermally grown ZnO NRs is neglected as well as Au NP-coating along the surfaces of those NRs, a clear trend with increasing HV (and electron-sample interaction volume) is visible: while at 3 kV, the energy of the primary electrons is completely dumped in a single ZnO NR, at 10 kV, the interaction volume of the electron-beam with the ZnO is extended to an extent where three or even more ZnO NRs can easily be excited. Taken into account that the angular distribution of the hydrothermally grown ZnO NRs can be as large as 60° rather than normal to the substrate surface as shown in Fig. 7, the increased electron-sample interaction volume at 10 kV, particularly in the lateral direction, allows for

TABLE 1: UV enhancement factors for Au NP-coated ZnO NRs and *a*-plane ZnO bulk crystal at three different acceleration voltages collected at 10 K.

HV (kV)	ZnO NR UV enhancement	*a*-plane ZnO UV enhancement
3	1.8	N/A
5	3.6	2.0
10	5.1	1.4
15	N/A	1.4

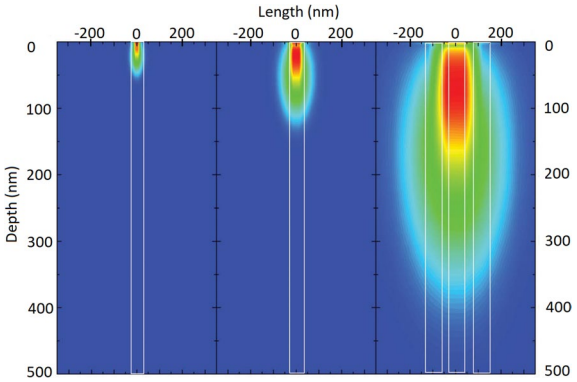

Figure 7: Monte Carlo simulation (CASINO) of the energy loss within ZnO coated with a thin Au film at 3 kV (left), 5 kV (center) and 10 kV (right). The white lines represent the outlines of the typical ZnO NR with a diameter of 40 nm. For simplicity, the ZnO NRs have been vertically oriented, not reflecting the actual alignment used in the experiment.

the excitation of substantially greater NR surface area than at 3 kV. Since the interaction between the Au NPs with the excitons in ZnO is largest at their interface, the irradiation of a larger surface area coated with Au NPs results in an overall increased CL-UV enhancement.

Naturally, this effect can only occur in non-aligned ZnO NRs as (i) the Au NP-coated surfaces are more randomly distributed with respect to the optical excitation source, and (ii) the deposition of a uniform Au NP surface coating reaching down to the bottom of the ZnO NRs is more likely to be achieved without shadowing effects. The other side of the argument is that a planar ZnO structure coated with Au NPs should exhibit a lower UV enhancement factor, potentially close to that of the Au NP-coated ZnO NRs at 3 kV (Table 1). Furthermore, a decrease in UV enhancement factor with increasing HV is expected due to the larger electron-beam interaction volume within the bulk crystal as the interaction between Au NPs and ZnO is largest to their interface. We therefore repeat the CL measurements of an *a*-plane ZnO single crystal, half coated with an identical Au NP surface coating. The results are shown in Fig. S2 and summarized in Table 1, revealing that the highest UV enhancement factor is found at the lowest HV with a maximum of 2, confirming the hypothesis that the use of a high angular distribution of NRs is beneficial for a surface coating-mediated light emission enhancement in comparison to a planar structure.

Conclusions

High-density ZnO NR arrays on Si substrates were hydrothermally grown at low temperature between 70 and 100 °C using a ZnO seed layer. The effect of different seed layer deposition methods on the alignment and morphology of ZnO NRs was studied, indicating that the coverage of the seeds over the substrate is directly related to the NR coverage as well as their alignment with respect to the substrate normal. Notably, the ZnO seed diameter did not have a strong effect on the diameter of the resulting ZnO NRs using the drop-casting method, while the dimensions of sputter-coated ZnO seeds were found to directly translate to the diameter of the NRs. In addition, the results of a systematic study of the effects of both the growth temperature and the growth time, ranging from two to four hours, suggests that neither the length nor the diameter of the ZnO NRs can be reliably controlled by varying these growth parameters using a hydrothermal ZnO NR fabrication route. Nevertheless, the low temperature hydrothermal growth process is demonstrated to be facile and cost-effective approach that reliably produces large areas of crisscross-aligned hexagonal ZnO NRs with a relatively small NR diameter in the range of 20–60 nm and an approximate length of 600 nm. Significantly, the ZnO NRs can be grown with a controllable angular distribution with respect to the substrate normal by size and distribution of pre-growth sputter-coated seeds. This feature as well as the exceptionally high crystal and luminescence quality of the as-grown ZnO NRs may be useful for the wave-guided, angular light emission distribution for ZnO NR light-emitting devices as well as for ZnO NR sensor devices whose performance would benefit from a large surface area of non-polar, *m*-plane {01-10} ZnO with high component parallel to the substrate. Furthermore, the high angular distribution of the ZnO NRs have demonstrated to be highly beneficial for applications involving surface coatings and surface coating-mediated emission enhancement which make them a promising candidate for light-emitting or photovoltaic applications and devices, as both light injection and light extraction can be readily enhanced.

Methods

The ZnO NRs were prepared by a low temperature hydrothermal method [64]. Polished Si (110) wafers were used as growth substrate which were cleaned by a standard process consisting of consecutive ultrasonication steps in acetone, isopropanol and deionized water, each for 15 min. Subsequently, a ZnO seed layer was deposited by drop-casting 5 mM zinc acetate (> 98%, $(C_2H_3O_2)_2Zn^*2H_2O$) solution in ethanol followed by an annealing step at 250 °C in air for 20 min. This entire procedure was repeated several times. Alternatively, a thin layer of ZnO seeds was sputter-coated, using a high purity ZnO target, onto the clean Si substrate, using a home-built deposition chamber at a base pressure of 10^{-6} mbar and a sputtering pressure of 1.3×10^{-3} mbar, a DC power of 30 W and argon gas flow of 60 sccm. The ZnO NRs were grown by placing the ZnO seed layer-coated Si substrate upside down in an autoclave containing a mixture of 25 mM zinc nitrate hexahydrate (98%, $Zn(NO_3)_26H_2O$), and

25 mM hexamethylenetetramine (HMT, ≥ 99.0%, $C_6H_{12}N_4$), purchased from Sigma-Aldrich. The autoclave was held at 70–100 °C in a pre-heated conventional oven between 2 and 4 h before removing the substrates and rinsing them in de-ionized water. The autoclave was thoroughly cleaned after each growth cycle.

The chemical process of the equimolar ZnO NR growth can be described by the following reactions [25]:

$$C_6H_{12}N_4 + 6H_2O \rightarrow 6HCHO + 4NH_3$$

$$NH_3 + H_2O \rightarrow NH^{4+} + OH^-$$

$$2OH^- + Zn^{2+} \leftrightarrow Zn(OH)_2$$

$$Zn(OH)_2 \leftrightarrow ZnO + H_2O$$

A gold nanoparticle (NP) surface coating onto the as-grown ZnO NRs was produced by a simple two-step process. (1) A thin Au film of a nominal thickness of 1 nm was sputtered using a home-built deposition chamber with a base pressure of 1.2×10^{-3} mbar at DC power of 30 W and argon gas flow of 60 sccm. (2) Subsequent annealing at 300 °C for 30 min was carried out in a tube furnace. The uniform Au NP-coating with an average NP diameter of 5 nm can be seen in Fig. S1. Each sample was only coated half with Au NPs, leaving the other half as a reference.

The morphology and size of the ZnO NR samples were studied and measured with a Zeiss Supra 55VP Field Emission Scanning Electron Microscope. Secondary electron (SE) SEM images were collected using an acceleration voltage of 10 kV. The 325 nm line of a Melles Griot He–Cd laser with a power of 2.1 mW was coupled into the chamber of an FEI Quanta 200 SEM equipped with a liquid helium cold stage, allowing for concurrent collection of photoluminescence (PL) and cathodoluminescence (CL) spectra. CL and PL emitted from the sample was collected by a parabolic mirror and analyzed using an Ocean Optics QE Pro spectrometer and an Oriel MS257 1/4 m imaging spectrograph equipped with a Hamamatsu S7011-1007 CCD (high-resolution of below 0.1 nm). All spectra were corrected for the total system response. A detailed comparison of CL and PL spectroscopy of Au-coated ZnO NRs has been provided in previous work [46]. X-ray diffraction (XRD) was conducted using a Siemens D5000 diffractometer using Cu Kα radiation at a scanning step of 0.02°.

Acknowledgments

The authors would like to thank Geoff McCredie and Katie McBean for technical support, as well as Dr. Olivier Lee Cheong Lem for fruitful discussions. This project was funded by the Australian Research Council Discovery Projects DP150103317 and DP210101146.

Funding

Open Access funding enabled and organized by CAUL and its Member Institutions.

Data availability

Data reported in the manuscript will be made available upon reasonable request.

Declarations

Conflict of interest The authors declare that there are no conflict of interest related to this paper.

Open Access

Supplementary Information

The online version contains supplementary material available at https://doi.org/10.1557/s43578-023-00941-x.

References

1. D.G. Thomas, The exciton spectrum of zinc oxide. J. Phys. Chem. Solids **15**, 86–96 (1960)
2. C. Klingshirn, ZnO: from basics towards applications. Phys. Status Solidi (b) **244**, 3027–3073 (2007)
3. Ü. Özgür et al., A comprehensive review of ZnO materials and devices. J. Appl. Phys. **98**, 041301 (2005)
4. A.B. Djurišić, Y.H. Leung, Optical properties of ZnO nanostructures. Small **2**, 944–961 (2006)
5. P.K. Aspoukeh, A.A. Barzinjy, S.M. Hamad, Synthesis, properties and uses of ZnO nanorods: a mini review. Int. Nano Lett. **12**, 153–168 (2022)

6. S. Anantachaisilp et al., Tailoring deep level surface defects in ZnO nanorods for high sensitivity ammonia gas sensing. J. Phys. Chem. C **118**, 27150–27156 (2014)
7. M. Willander, *Zinc Oxide Nanostructures: Advances and Applications* (Pan Stanford Publishing, Redwood City, 2014)
8. A.B. Yadav, P.V.L. Parvathi, S.R. Thabassum, Effect of precursor chemistry on the structural and sensing properties of hydrothermally grown nanorods. Appl. Phys. A **125**, 446 (2019)
9. A.B. Yadav, P.V.L. Parvathi, R.T. Shaik, Zero bias UV detection and precursor effect on properties of ZnO nanorods grown by hydrothermal method on SiO_2/p-Si substrate. Thin Solid Films **685**, 343–352 (2019)
10. P. Gu, X. Zhu, D. Yang, Vertically aligned ZnO nanorods arrays grown by chemical bath deposition for ultraviolet photodetectors with high response performance. J. Alloys Compd. **815**, 152346 (2020)
11. Y. Ji et al., Ultraviolet photodetectors using hollow p-CuO nanospheres/n-ZnO nanorods with a pn junction structure. Sens. Actuators A **304**, 111876 (2020)
12. J. Huang et al., Visible light-activated room temperature NH_3 sensor base on CuPc-loaded ZnO nanorods. Sens. Actuators B **327**, 128911 (2021)
13. S.M. Mohammad et al., Ultraviolet electroluminescence from flowers-like n-ZnO nanorods/p-GaN light-emitting diode fabricated by modified chemical bath deposition. J. Lumin. **226**, 117510 (2020)
14. H. Wang et al., N-pentanol sensor based on ZnO nanorods functionalized with Au catalysts. Sens. Actuators B **339**, 129888 (2021)
15. N.H. Alvi, K. Ul Hasan, O. Nur, M. Willander, The origin of the red emission in n-ZnO nanotubes/p-GaN white light emitting diodes. Nanoscale Res. Lett. **6**, 1–7 (2011)
16. I.C. Robin et al., Evidence for low density of nonradiative defects in ZnO nanowires grown by metal organic vapor-phase epitaxy. Appl. Phys. Lett. **91**, 143120 (2007)
17. S. Nicolay, S. Faÿ, C. Ballif, Growth model of MOCVD polycrystalline ZnO. Cryst. Growth Des. **9**, 4957–4962 (2009)
18. H. Zheng et al., Electrochemical deposition of ZnO nanowire arrays: organization, doping, and properties. Sci. Adv. Mater. **2**, 336–358 (2010)
19. K.N. Hui et al., Enhanced light extraction efficiency of GaN-based LED with ZnO nanorod grown on Ga-doped ZnO seed layer. ECS Solid State Lett. **2**, Q43–Q46 (2013)
20. L.E. Greene et al., Low-temperature wafer-scale production of ZnO nanowire arrays. Angew. Chem. Int. Ed. **42**, 3031–3034 (2003)
21. J.X. Wang et al., Hydrothermally grown oriented znO nanorod arrays for gas sensing applications. Nanotechnology **17**, 4995–4998 (2006)
22. J. Qiu et al., The growth mechanism and optical properties of ultralong ZnO nanorod arrays with a high aspect ratio by a preheating hydrothermal method. Nanotechnology **20**, 155603 (2009)
23. A.R. Azulay, Y. Turkulets, D.D. Gaudio, R.S. Goldman, I. Shalish, Why do nanowires grow with their c-axis vertically-aligned in the absence of epitaxy? Sci. Rep. **10**, 6554 (2020)
24. S. Bai et al., High-performance integrated ZnO nanowire UV sensors on rigid and flexible substrates. Adv. Funct. Mater. **21**, 4464–4469 (2011)
25. V. Gerbreders et al., Hydrothermal synthesis of ZnO nanostructures with controllable morphology change. CrystEngComm **22**, 1346–1358 (2020)
26. R.B.M. Cross, M.M.D. Souza, E.M.S. Narayanan, A low temperature combination method for the production of ZnO nanowires. Nanotechnology **16**, 2188–2192 (2005)
27. C.B. Tay, H.Q. Le, S.J. Chua, K.P. Loh, Empirical model for density and length prediction of ZnO nanorods on GaN using hydrothermal synthesis. J. Electrochem. Soc. **154**, K45 (2007)
28. Y. Iqbal, M.K. Mustafa, J. Wang, C. Wang, Orientation and actual growth mechanism of ZnO nanorods through hydrothermal method on gold seed layer. AIP Adv. **11**, 125006 (2021)
29. K. Takanezawa, K. Hirota, Q.-S. Wei, K. Tajima, K. Hashimoto, Efficient charge collection with ZnO nanorod array in hybrid photovoltaic devices. J. Phys. Chem. C **111**, 7218–7223 (2007)
30. H. Wang, J. Xie, K. Yan, M. Duan, Growth mechanism of different morphologies of ZnO crystals prepared by hydrothermal method. J. Mater. Sci. Technol. **27**, 153–158 (2011)
31. S. Xu, C. Lao, B. Weintraub, Z.L. Wang, Density-controlled growth of aligned ZnO nanowire arrays by seedless chemical approach on smooth surfaces. J. Mater. Res. **23**, 2072–2077 (2008)
32. R. Nandi, R.S. Srinivasa, S.S. Major, Morphology and photoluminescence of ZnO nanorods grown on sputtered GaN films with intermediate ZnO seed layer. Mater. Chem. Phys. **182**, 155–166 (2016)
33. S. Al-lami, H. Jaber, Controlling ZnO nanostructure morphology on seedless substrate by tuning process parameters and additives. Chem. Mater. Res. **6**, 101–109 (2014)
34. L.L. Yang, Q.X. Zhao, M. Willander, Size-controlled growth of well-aligned ZnO nanorod arrays with two-step chemical bath deposition method. J. Alloys Compd. **469**, 623–629 (2009)
35. Y. Liu et al., Field emission properties of ZnO nanorod arrays by few seed layers assisted growth. Appl. Surf. Sci. **331**, 497–503 (2015)
36. K. Gautam, I. Singh, P.K. Bhatnagar, K.R. Peta, The effect of growth temperature of seed layer on the structural and optical properties of ZnO nanorods. Superlattices Microstruct. **93**, 101–108 (2016)

37. N.T. Son, J.-S. Noh, S. Park, Role of ZnO thin film in the vertically aligned growth of ZnO nanorods by chemical bath deposition. Appl. Surf. Sci. **379**, 440–445 (2016)
38. J. Song, S. Lim, Effect of seed layer on the growth of ZnO nanorods. J. Phys. Chem. C **111**, 596–600 (2007)
39. D. Byrne et al., A study of drop-coated and chemical bath-deposited buffer layers for vapor phase deposition of large area, aligned, zinc oxide nanorod arrays. Cryst. Growth Des. **10**, 2400–2408 (2010)
40. E.J. Guidelli, O. Baffa, D.R. Clarke, Enhanced UV emission from silver/ZnO and Gold/ZnO core-shell nanoparticles: photoluminescence, radioluminescence, and optically stimulated luminescence. Sci. Rep. **5**, 14004 (2015)
41. J. Lu et al., Improved UV photoresponse of ZnO nanorod arrays by resonant coupling with surface plasmons of Al nanoparticles. Nanoscale **7**, 3396–3403 (2015)
42. N. Joshi et al., UV-assisted chemiresistors made with gold-modified ZnO nanorods to detect ozone gas at room temperature. Microchim. Acta **186**, 418 (2019)
43. Q.K. Doan et al., Enhanced optical properties of ZnO nanorods decorated with gold nanoparticles for self cleaning surface enhanced Raman applications. Appl. Surf. Sci. **505**, 144593 (2020)
44. F. Zhou et al., Electrodeposition of gold nanoparticles on ZnO nanorods for improved performance of enzymatic glucose sensors. Mater. Sci. Semicond. Process. **105**, 104708 (2020)
45. S. Fiedler et al., Correlative study of enhanced excitonic emission in ZnO coated with Al nanoparticles using electron and laser excitation. Sci. Rep. **10**, 2553 (2020)
46. S. Fiedler, L.O. Lee Cheong Lem, C. Ton-That, A. Hoffmann, M.R. Phillips, Enhancement of the UV emission from gold/ZnO nanorods exhibiting no green luminescence. Opt. Mater. Express **10**, 1476 (2020)
47. S. Fiedler, L.O. Lee Cheong Lem, C. Ton-That, M.R. Phillips, The role of surface depletion layer effects on the enhancement of the UV emission in ZnO induced by a nanostructured Al surface coating. Appl. Surf. Sci. **504**, 144409 (2020)
48. N. Gogurla, A.K. Sinha, S. Santra, S. Manna, S.K. Ray, Multifunctional Au-ZnO plasmonic nanostructures for enhanced UV photodetector and room temperature NO sensing devices. Sci. Rep. **4**, 6483 (2014)
49. V. Perumal et al., Characterization of gold-sputtered zinc oxide nanorods—a potential hybrid material. Nanoscale Res. Lett. **11**, 31 (2016)
50. W. Chamorro et al., Local structure-driven localized surface plasmon absorption and enhanced photoluminescence in ZnO-Au thin films. J. Phys. Chem. C **120**, 29405–29413 (2016)
51. H.J. Jung et al., Low-temperature hydrothermal growth of ZnO nanorods on sol–gel prepared ZnO seed layers: optimal growth conditions. Thin Solid Films **524**, 144–150 (2012)
52. L. Zhu, M.R. Phillips, C. Ton-That, Coalescence of ZnO nanowires grown from monodisperse Au nanoparticles. CrystEngComm **17**, 4987 (2015)
53. R. Idiawati et al., Effect of growth time on the characteristics of ZnO nanorods. IOP Conf. Ser.: Mater. Sci. Eng. **202**, 012050 (2017)
54. O. Černohorský et al., Modeling of solution growth of ZnO hexagonal nanorod arrays in batch reactors. Cryst. Growth Des. **20**, 3347–3357 (2020)
55. E.S. Babu, S.-K. Hong, T.S. Vo, J.-R. Jeong, H.K. Cho, Photoelectrochemical water splitting properties of hydrothermally-grown ZnO nanorods with controlled diameters. Electron. Mater. Lett. **11**, 65–72 (2015)
56. S. Guillemin et al., Critical nucleation effects on the structural relationship between ZnO seed layer and nanowires. J. Phys. Chem. C **116**, 25106–25111 (2012)
57. S.-W. Chen, J.-M. Wu, Nucleation mechanisms and their influences on characteristics of ZnO nanorod arrays prepared by a hydrothermal method. Acta Mater. **59**, 841–847 (2011)
58. M.R. Wagner, Fundamental properties of excitons and phonons in ZnO: a spectroscopic study of the dynamics, polarity, and effects of external fields, Doctoral dissertation, Technical University Berlin, Germany (2010)
59. B.P. Zhang et al., Phonon replica of free excitons in Zno epitaxial films. Nonlinear Opt. (Mclc) Sect. B **29**, 621–627 (2002)
60. S. Anantachaisilp et al., Nature of red luminescence in oxygen treated hydrothermally grown zinc oxide nanorods. J. Lumin. **168**, 20–25 (2015)
61. S. Choi et al., Photophysics of point defects in ZnO nanoparticles. Adv. Opt. Mater. **3**, 821–827 (2015)
62. C. Ton-That, L. Weston, M.R. Phillips, Characteristics of point defects in the green luminescence from Zn- and O-rich ZnO. Phys. Rev. B **86**, 115205 (2012)
63. D. Drouin et al., CASINO V2.42—a fast and easy-to-use modeling tool for scanning electron microscopy and microanalysis users. Scanning **29**, 92–101 (2007)
64. L.E. Greene et al., General route to vertical ZnO nanowire arrays using textured ZnO seeds. Nano Lett. **5**, 1231–1236 (2005)